Journal of Materials Chemistry C

Accepted Manuscript

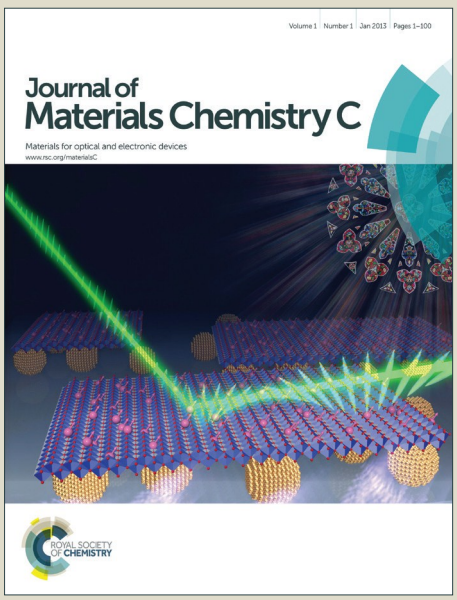

ROYAL SOCIETY OF CHEMISTRY

www.rsc.org/materialsC

Journal Name

RSCPublishing

Cite this: DOI: 10.1039/x0xx00000x

Fluoranthene Derivatives as Blue Fluorescent Materials for Non-doped Organic Light-Emitting Diodes

Shiv Kumar[a], Deepak Kumar [a], Yogesh Patil[b], and Satish Patil[*a]

Received 00th January 2012,
Accepted 00th January 2012

DOI: 10.1039/x0xx00000x

www.rsc.org/

In this study, we report synthesis of symmetrically and non-symmetrically functionalized fluoranthene-based blue fluorescent molecular materials for non-doped electroluminescent devices. The solid state structure of these fluorophores has been established by single crystal X-ray diffraction analysis. Furthermore, a detailed experimental and theoretical study has been performed to understand the effect of symmetric and non-symmetric functional groups substitution on optical, thermal and electrochemical properties of fluoranthene. These materials exhibit a deep blue emission and high PLQY in solution and solid state. The vacuum deposited, non-doped electroluminescent devices with device structure: ITO/NPD (15 nm)/CBP (15 nm)/EML (40 nm)/TPBI (30 nm)/LiF (1 nm)/Al were fabricated and characterized. A systematic shift in peak position of EL emission was observed from sky blue to bluish-green with EL maxima from 477 nm to 490 nm due to different functional groups on periphery of fluoranthene. In addition, a high luminance of ≥ 2000 cd/m^2 and encouraging external quantum efficiency (EQE) of 1.1-1.4 % was achieved. A correlation of molecular structure with device performance has been established.

Introduction

In 1963, Pope and co-workers reported the first observation of electroluminescence in anthracene single crystals at an applied dc voltage of more than 400 V across the two electrodes.[1] However, organic light-emitting diodes (OLEDs) operating at such high driving voltage were of no commercial use, but this work has stimulated very intense topic of research in the field of OLED. Numerous efforts have been made to understand the electroluminescence phenomena in organic crystals and fabrication of OLEDs for practical applications.[2,3] In 1987, Tang and Van Slyke at Eastman Kodak successfully demonstrated a highly efficient electroluminescent device using organic material operating at a voltage below 10 V, since then OLEDs have attracted considerable scientific and industrial interests.[4] At present, numerous research groups and display manufacturing companies are working closely to develop OLED materials and technology for commercial applications such as flat-panel displays and solid-state lighting.[5-7] In order to achieve a full-color display, it requires three primary colors *viz.* blue, green and red; of equal efficiency, stability, and color purity.[8] However, the achievement of stable and efficient blue emission is still challenging compared to green and red emission due to requirement of wide band gap materials and high operating voltage.[9] To obtain highly efficient OLEDs with low operational voltage, devices usually require complex configurations with several additional layers sandwiched between two electrodes to ease the charge injection and transport along with effective exciton confinement.[10, 11] In this regard, blue OLEDs device fabrication process is tedious, complicated and exorbitant to compete with other flat-display technologies. In order to simplify the device configuration, many multifunctional materials have been developed possessing the characteristics such as high luminescence and charge injection/transporting property.[12,13] The utilization of such multifunctional materials and simplified device configuration may reduce the overall cost of OLEDs significantly.[14] In addition, it has been observed that most of the blue fluorescent materials such as anthracene,[15] fluorene,[16] spiro,[17] truxene,[18] and pyrene[19] show very high photoluminescence quantum yield (PLQY) in dilute solution while their fluorescence gets significantly quenched in solid state due to self-aggregation. In order to avoid aggregation effect, these fluorophores were used as guest in host matrix with optimized charge transport and luminescent properties in OLEDs.[20] Such guest-host emitter doped systems not only improve the efficiency and operational stability of the device by confining and transferring the electrical excitons to highly emissive and stable dopant in host matrix, but also minimize the undesired processes such as non-radiative pathways.[21-23] Although the guest-host systems can improve the device efficiency significantly, but the intrinsic phase separation could deteriorate the performance severely during the operation.[24]

Such guest-host systems require suitable hosts which could confine the dopants effectively. The aforementioned limitations with guest-host emitter system led to tremendous efforts to circumvent the issue by using non-doped emitters in OLEDs.[16, 25,26] Intrigued by the good photoluminescence properties of the blue fluorophores in dilute solution, substantial effort have been devoted to develop deep-blue emitters with reduced fluorescence quenching in solid state. In pursuance of non-planar molecular structures with reduced inter-molecular interactions in solid state, various research groups used the strategy of introduction of rigid and bulky substituents such as phenyl, naphthyl, and *tert*-butyl groups at the periphery of the fluorophores. For example, Kwon *et al.* successfully introduced rigid and bulky substituent such as tetraphenylsilane to the 9,10-positions of the anthracene,[27] and the resulting non-planar anthracene derivative not only exhibited the photophysical properties similar to the pristine 9,10-diphenylanthracene (DPA) due to suppression of the intermolecular interactions in thin film and short π-conjugation length, but also exhibited a high glass transition temperature (T_g). Along with anthracene, fluorene derivatives have been widely investigated and explored as deep blue emitting materials for OLEDs due to their high PLQYs and thermal stability.[16] However, the green emission band is observed in fluorene based OLEDs, originates from fluorenone defects due to oxidation at the methane bridge and results into poor color purity and fluorescence quenching.[28] Nevertheless, Wong *et al.* suggested a methods of stabilizing the blue emission of polyfluorenes, by rational design and synthesis of ter(9,9-diarylfluorene), in which the *C9*-position was substituted by aryl substituents to impede the oxidation process.[29]

Similar to fluorine family, fluoranthene is very attractive fluorophore. The rigid planarized biphenyl structure in the fluoranthene unit leads to a wide band-gap with blue emission and also provides thermal and electrochemical stability. These properties make fluoranthene an interesting material for optoelectronics devices.[30-33] Besides theoretical studies, enormous efforts have been made to develop the facile synthesis of fluoranthene derivatives.[34] The interesting properties such as wide band gap, high PLQY, thermal and electrochemical stability make fluoranthene derivatives as potential candidate for blue organic light-emitting diodes.[35-41] By considering these advantages of fluoranthene, this work reports design and synthesis of highly arylated, symmetrically and non-symmetrically functionalized fluoranthene derivatives for non-doped electroluminescent devices. By substituting different functional groups on the periphery of fluoranthene, we investigated their differences in solid-state packing and photophysical properties. The fluorophores were found to give deep-blue emissions with high fluorescent quantum yield. OLED fabricated using these materials were observed to deliver moderate external quantum efficiency with sky blue to bluish-green emission.

Results and discussion

Synthesis

The general route for synthesis of fluoranthene derivatives is outlined in Scheme 1. The intermediate, 7,9-diphenyl-8*H*-cyclopenta[a]acenaphthylen-8-one (DPC) was synthesised by a double Knoevenagel condensation of 1,3-diphenylpropanone and acenenaphthenequinone described by Walker *et al,* to form a dark brown solid.[42] Various symmetrically and non-symmetrically functionalized acetylene derivatives were synthesised by palladium-catalysed Sonogashira coupling reaction.[43] The desired fluoranthene derivative was synthesized via Diels-Alder cycloaddition reaction of acetylene derivatives with DPC in diphenyl ether as solvent in a sealed tube. After removing the diphenyl ether under reduced pressure, the resultant products were isolated by column chromatography in the quantitative yield of 60-70%. All the compounds were readily soluble in common organic solvents such as dichloromethane, chloroform, tetrahydrofuran, and toluene but sparingly soluble or insoluble in methanol and acetonitrile.

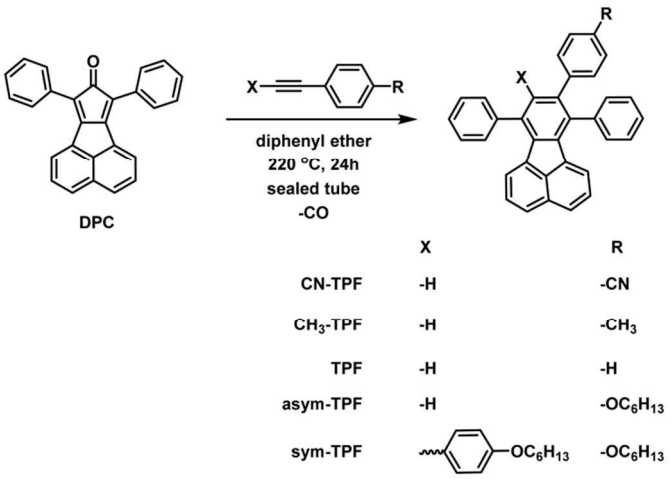

Scheme 1: Synthetic route for preparation of fluoranthene derivatives

Single Crystal X-ray Diffraction Analysis

Several attempts were made to grow high quality crystals using various organic solvent mixtures for single crystal X-ray analysis. The single crystals for diffraction studies were obtained by slow solvent evaporation method in dichloromethane/ethanol mixtures at ambient temperature. All the crystals were transparent in nature and bright greenish-yellow in color. The single crystal data were collected at room temperature unless mentioned otherwise. The crystal structures were established by subsequent refinement of the collected data and the crystal packing was analysed. All the compounds crystallized in monoclinic space group $P2_1/c$ except the compound asym-TPF which crystallized in triclinic space group *P*-1. The ORTEP diagram of crystal structures are shown in Figure 1. Since, all the fluoranthene derivatives have common fluoranthene core as backbone with no conformational flexibility; the variations in structural arrangements observed in

the solid state are purely governed by variations of the substituents on phenyl rings. Furthermore, the steric repulsion between aryl rings at the periphery of fluoranthene unit prevents these compounds to adopt a planar structure. The degree of torsion angle between fluoranthene unit and phenyl ring is influenced by the number of aryl substitutions. The crystal structure of non-symmetrically functionalized fluoranthene derivatives CN-TPF, TPF, and CH_3-TPF were found to be isostructural but differ in molecular assembly and intermolecular interactions due to variation in functional group on the phenyl ring. The selective crystallographic details of all compounds are summarized in Table S1 (ESI). The compound TPF without functional group has been considered as the reference to compare the effect of functional group on the molecular structure and the solid state packing of fluorophores. The presence of symmetric phenyl rings at C13, C16 positions and an unsymmetrical phenyl ring at C15-position of fluoranthene creates large steric hindrance resulting in weak π-π interactions and variation in torsional angles.

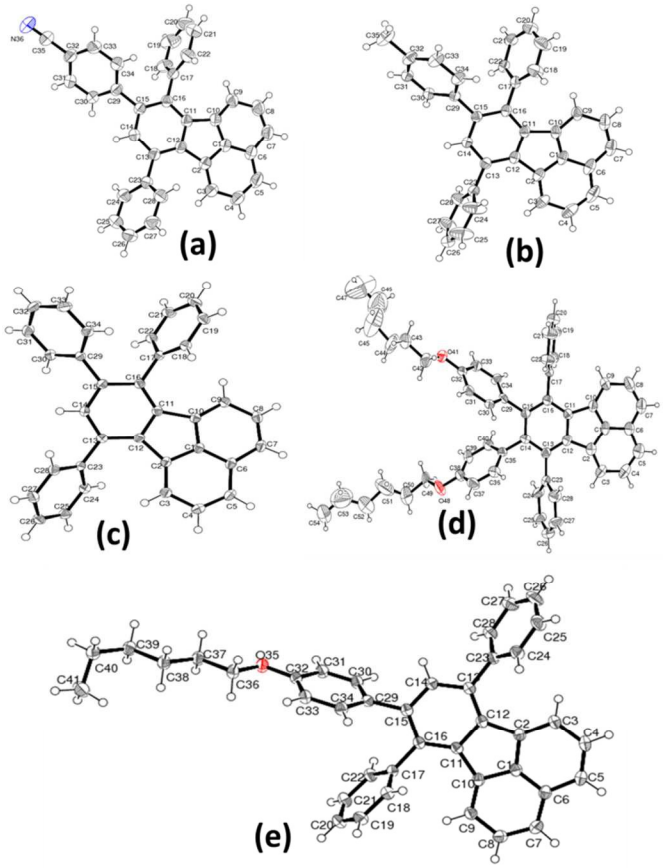

Figure 1: ORTEP diagram of crystal structures of fluoranthene derivatives

The structures vary in the torsional angle at C13, C16 and C15 position (ESI Table S2). The supramolecular assembly was stabilized by C–H•••π and C–H•••N/O interactions as shown in Figure S16 (ESI). Additionally, stacking has been observed in case of CH_3-TPF molecules. In case of sym-TPF structure, we observed the presence of diethyl ether and water in the crystal lattice. The structure was refined by squeezing these solvent molecules with PLATON squeeze. The refinement details are embedded in the CIF file. The selective crystallographic details of all compounds are summarized in Table 1.

Thermal Properties

Thermal properties and stability of the compounds were investigated by differential scanning calorimetry (DSC) and thermogravimetric analysis (TGA). In DSC curves (Figure 2), we observed these compounds exhibit amorphous material behaviour except CH_3-TPF, which shows crystalline nature. The thermal properties of these compounds can be corroborated with the molecular structure and various types of interactions in the solid state. For comparison, we consider TPF as reference without any functional group at the periphery. In solid state, the molecules of TPF compound held together purely by C–H•••π (2.685 Å) interactions, therefore it exhibit intermediate melting temperature (T_m) of 191 °C. In case of the compound CN-TPF which shows a 44 °C higher T_m than the compound TPF, the molecules are stabilized by C–H•••N interactions in addition to C–H•••π interactions in solid state. The highest T_m of 260 °C and crystalline nature displayed by the compound CH_3-TPF is attributed to the C–H•••π and π•••π stacking interactions among the neighbouring molecules. The compound asym-TPF shows a lower T_m than the compound TPF due to presence of flexible hexylkoxy chain. The van der Waals interactions between hexylkoxy chains and C–H•••O interactions hold the molecules together in the solid state. The lowest T_m of 90 °C exhibited by the compound sym-TPF attributed to the presence of two flexible hexylkoxy chains. It was interesting to observe the splitting of the T_m peak in the DSC curve and this splitting may be due to first melting of the two flexible hexylkoxy chains followed by collapse of the self-assembly. From TGA curves (Figure 2), all the compounds were found to be stable in the range of 260-305 °C and the stability of the compound strongly depends on the nature of the functional group at the periphery. The summary of the thermal properties is given in the Table 2.

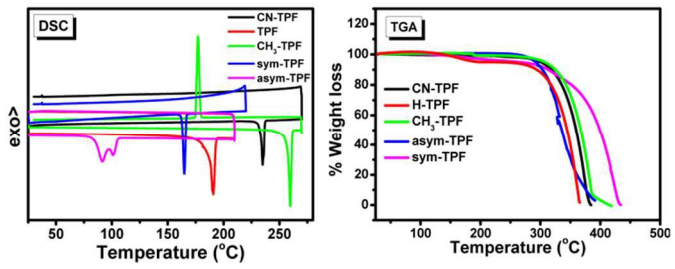

Figure 2: Thermal properties of fluoranthene derivatives. DSC trace (left), TGA thermogram (right) (scan rate 5 °C/min)

Electrochemical properties

The cyclic voltammograms of ferrocene and studied compounds are shown in Figure S17 (ESI). The oxidation onsets of ferrocene, CN-TPF, TPF, CH_3-TPF, asym-TPF, and sym-TPF were observed at 0.25 V, 1.48 V, 1.40 V, 1.40 V, 1.36 V, and 1.22 V, respectively, from their corresponding CV

curves. A gradual decrease in the oxidation potential was observed from the compound CN-TPF to sym-TPF as the electron donating strength increased. All the compounds show the irreversible oxidation cycle. In case of reduction cycle, the compound asym-TPF and sym-TPF show pseudo-reversible nature. The reduction onsets of CN-TPF, TPF, CH_3-TPF, asym-TPF, and sym-TPF were observed at -1.78 V, -1.77 V, -1.67 V, -1.74 V, and 1.78 V, respectively. Hence, calculated electrochemical band gap was found to be in the range of 3.01-3.26 eV. The energy of HOMO and LUMO level calculated with respect to the Fc/Fc^+ couple is summarized in Table 1.

Table 1 Summary of electrochemical properties.

Compound	E_{ox} (V)	HOMO (eV)	E_{red} (V)	LUMO (eV)	E_g (eV)
CN-TPF	1.48	-6.03	-1.78	-2.77	3.26
TPF	1.40	-5.95	-1.77	-2.78	3.17
CH_3-TPF	1.40	-5.95	-1.67	-2.88	3.07
asym-TPF	1.36	-5.91	-1.74	-2.81	3.01
sym-TPF	1.22	-5.77	-1.78	-2.77	3.00

Photophysical Properties

The photophysical properties of these compounds were studied with UV-visible absorption and fluorescence spectroscopy (Figure 3(a) & (c)). In solution, the symmetrically and non-symmetrically functionalized compounds exhibit two well-resolved intense absorption bands at ~300±2 nm and ~375±2 nm and a well resolved peak at 329 nm as shown in Figure 3(a), which are attributed to π→π* transitions. The weak absorption band at ~375 nm exhibit low oscillator strength with broad shoulder at ~425 nm. There was no significant shift observed in the position of absorption maxima for all the compounds, suggesting that phenyl rings substituted on periphery of fluoranthene core do not participate in the extension of the π-conjugation due to steric hindrance. This also implies that the influence of the functional group on ground state is negligible. However, a gradual red shift in emission peak was observed from 449 nm to 478 nm as the electron donating strength of the functional group is increased from CN-TPF to sym-TPF. Further, this gradual shift is more pronounced in thin film. In neat films, a similar absorption pattern was observed with two well-resolved absorption bands at ~300±2 nm and ~382±2 nm along with broadening and red shift of ~5 nm of the absorption band at the longer wavelength as shown in Figure 3(c). The appearance of red shifted and broad absorption spectrum is due to strong intermolecular interactions and delocalization of π-electrons among neighbouring molecules in the solid state. Like the emission in solution, the emission maxima vary from ~455 nm to ~475 nm for CN-TPF to sym-TPF. From the low energy onset of the absorption bands in neat film, the optical band gaps were calculated by empirical equation ($E_g^{Optical}$=1240/λ_{onset}). The optical band gaps were found to be 3.0 eV and show small variations, depending on the nature of substituents. The energy gap calculated from absorption onset is well corroborated with the experimentally estimated values by CV, discussed in earlier section.

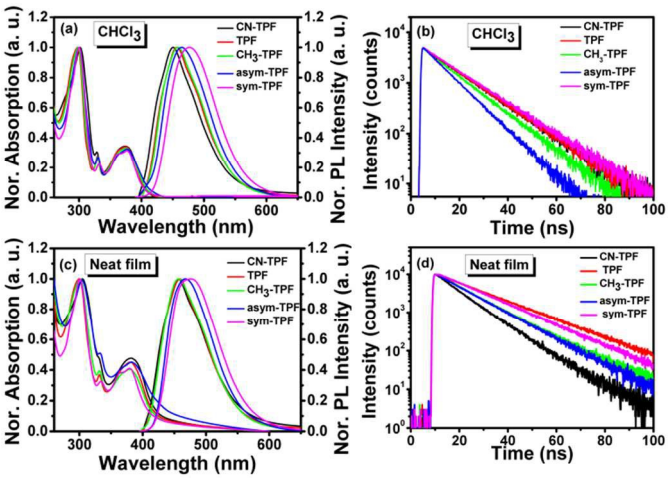

Figure 3: (a) Absorption and emission spectra, (b) PL decay profiles of fluoranthene derivatives in solution. (c) Absorption and emission spectra, (d) PL decay profiles of fluoranthene derivatives in neat films

Table 2 Summary of photophysical properties and thermal properties.

Compound	solution				neat film				E_g (eV)	T_m	T_d
	λ_{abs} (nm)	λ_{em}(nm)	τ(ns)	φ	λ_{abs} (nm)	λ_{em}(nm)	τ(ns)	φ	film	(°C)	(°C)
CN-TPF	300, 329, 376	449	13	0.57	301, 329, 380	455	10	0.42	3.10	235	300
TPF	295, 329, 375	456	13	0.72	299, 329, 382	455	18	0.57	3.08	191	290
CH_3-TPF	298, 329, 375	463	11	0.73	301, 329, 380	456	13	0.57	3.03	260	306
asym-TPF	300, 329, 377	464	9	0.80	304, 329, 382	467	12	0.65	3.01	165	290
sym-TPF	300, 329, 376	478	14	0.68	301, 329, 380	476	16	0.53	3.00	90	260

The fluorescence quantum yield (Φ) of all the derivatives exhibits in the range of 0.57-0.80 and 0.42-0.65 in solution and neat films, respectively. High PLQY observed for all the derivatives in neat film, attributed to their molecular structure and solid state packing. As shown in Figure 1, the aryl rings at the periphery of fluoranthene unit prevents these compounds adopting a planar structure and undergo π-π stacking (Figure S16, ESI). Such strategy has been utilized an effective way to reduce concentration quenching in the fluorescent and phosphorescent dyes.[44,45] The fluorescence lifetime of these compounds in chloroform and neat film was measured by time correlated single photon counting (TCSPC) method and is found to be in the range of 9-14 ns and 10-18 ns, respectively, (Figure 3(b) and (d)). The longer fluorescence lifetime and decrease in PLQY in neat films is evidence for aggregation quenching. The pertinent results of photophysical and fluorescence lifetime data on effect of the functional group were analyzed and summarized in Table 2.

Computational Results

To analyze the electronic structures of fluoranthene derivatives, theoretical calculations were performed using density functional theory (DFT). It is well established that, the energy levels of the frontier molecular orbitals especially HOMO and LUMO as well as their spatial distribution play very crucial role in determining the optical and electrochemical properties. In this regard, we employed DFT to optimize the ground state geometry with M062X functional in conjunction with the 3-21G basis set. The extent of conjugation was assessed with electron density plots of the HOMO and LUMO of fluoranthene derivatives as shown in Figure 4. The orbital diagrams are plotted with the contour value of 0.02 a.u. The plots of the HOMO and LUMO of the present molecule have the typical π molecular orbital characteristics. From the molecular orbital analysis, we infer that the lowest lying singlet-singlet absorption as well as emission corresponds to the $\pi \rightarrow \pi^*$ transition. Figure 5 illustrates that HOMO is delocalized while LUMO is localised on the fluoranthene core with very significant density overlap. This density overlap explains the high PLQY of these compounds in solution and thin film. In case of sym-TPF compound, HOMO is localized on the aryl substituents at 8,9-positions, whereas LUMO is localized on the fluoranthene core similar to other compounds.

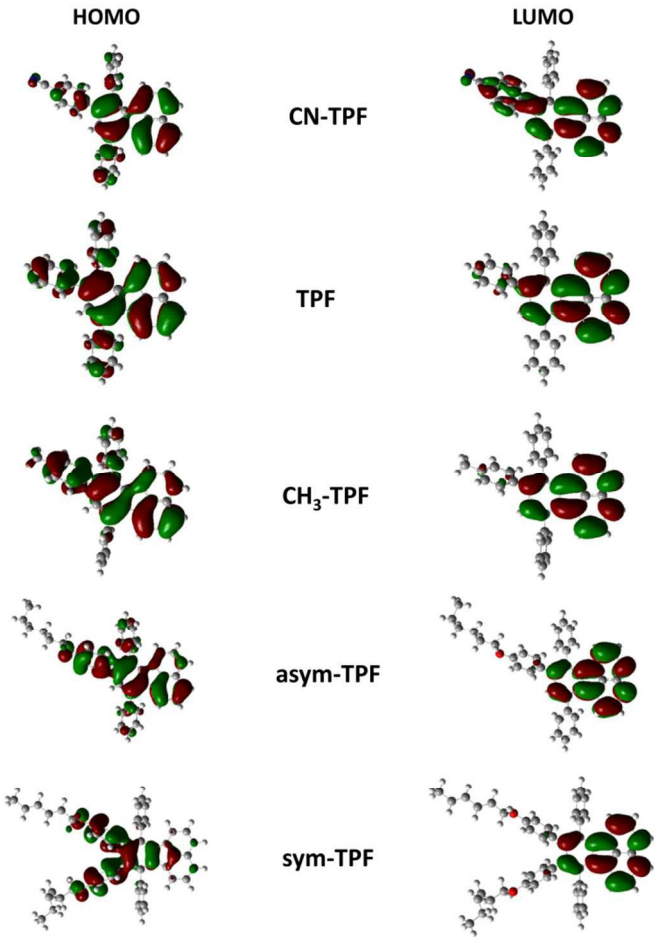

Figure 4: Frontier molecular orbitals of fluoranthene derivatives

Time-dependent DFT (TD-DFT) was employed to simulate the absorption spectra in gas phase and excited state geometry was optimized with M062X/3-21G level of theory. The simulated UV-visible spectra were found to be in very good agreement with the experimentally observed absorption spectra (ESI Figure S18). The selected key electronic transitions are summarized in (ESI Table S3).

Electroluminescence Characteristics

Electroluminescent characteristics were investigated by fabrication of a non-doped multilayer layer device comparing these compounds as light emitting layer with the following device configuration: ITO/NPD (15 nm)/CBP (25 nm)/EML (40 nm)/TPBi (30 nm)/LiF (1 nm)/Al, where NPD is *N,N′*-Di(*1*-naphthyl)-*N,N′*-diphenyl-(*1,1′*-biphenyl)-*4,4′*-diamine, CBP is *4,4′*-bis(*N*-carbazolyl)-*1,1′*-biphenyl, and TPBi is *2,2′,2″*-(*1,3,5*-Benzinetriyl)-tris(*1*-phenyl-*1*-*H*-benzimidazole), used as a hole-injecting, hole-transporting and electron transporting layer, respectively. The chemical structure, energy level diagram and device architecture is shown in Figure 5.

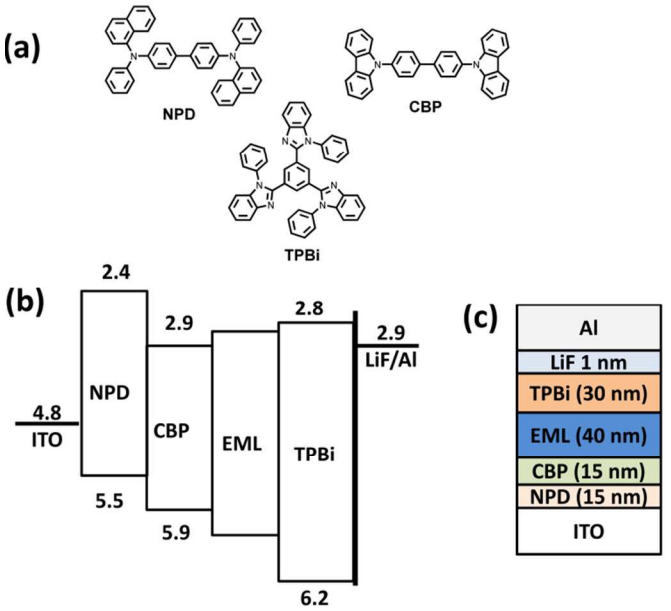

Figure 5: (a) Chemical structure of used materials (b) Energy level diagram, and (c) Device structure

Typical light emitting diode current density-voltage (J-V) and luminance-voltage (L-V) characteristics of fluoranthene based derivatives with the above mentioned device structure is shown in Figure 6(b) and (c), respectively. The turn-on voltage of the OLED was found to be 6.5 V, 7.3 V, 6.3 V, 6.8 V and 6.2 V with the maximum luminance of 5083 cd m^{-2}, 1067 cd m^{-2}, 4825 cd m^{-2}, 2723 cd m^{-2}, and 4148 cd m^{-2} for CN-TPF, TPF, CH_3-TPF, asym-TPF, and sym-TPF, respectively. The plot of external quantum efficiency-current density (EQE-J) is shown in Figure 6(d). All the devices showed the moderate EL performance with EQE in the range of 1.1 – 1.4 %. The CIE coordinates corresponding to EL spectra plotted in chromaticity diagram and luminance efficiency-luminance (LE-L) plot are shown in Figure S19 and S20 (ESI), respectively. A red shift was observed in EL spectra when compared with PL spectra, suggesting that the emission takes place from the interface of hole transport layer and emitting layer due to charge imbalance (Figure 6(a).). The EL properties are summarized in Table 3.

The device performance of fluorophores is strongly influenced by different functional groups. The compound TPF, asym-TPF and sym-TPF shows high efficiency roll-off, attributed to their low T_m and thermal stability. On the other hand, the compound CH_3-TPF and CN-TPF do not exhibit efficiency roll-off of the EL device. The low EQE for compound CN-TPF and TPF is attributed to their higher band gap (3.17 and 3.26 eV) and in particular CN-TPF also exhibit low PLQY compared to other four compounds.

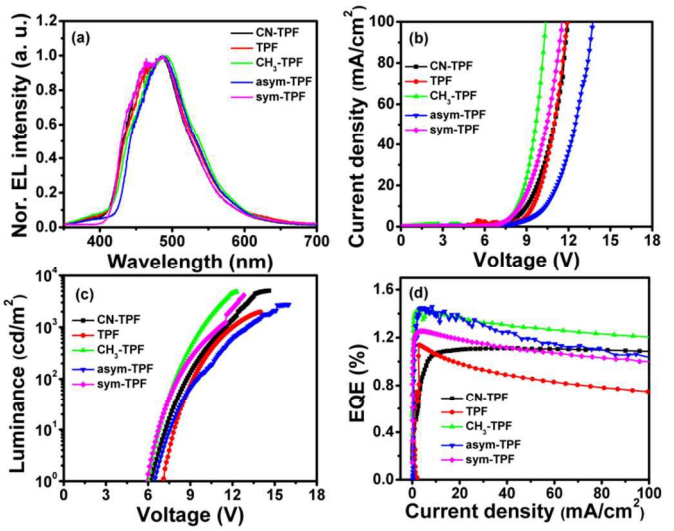

Figure 6: (a) EL spectra (b) J-V curve (c) L-V characteristics and (d) EQE-J plot.

Table 3 Summary of EL characteristics.

EML	EL (nm)	V_{on} (V)	L_{max} (cd/m^2)	LE (cd/A)	EQE (%)	CIE (x, y)
CN-TPF	477	6.2	5083	1.31	1.10	(0.13, 0.21)
TPF	487	7.1	1967	1.39	1.15	(0.13, 0.22)
CH_3-TPF	490	6.0	4825	1.79	1.45	(0.13, 0.25)
asym-TPF	487	6.2	2723	1.98	1.45	(0.13, 0.26)
sym-TPF	487	6.0	4148	1.59	1.25	(0.13, 0.27)

The performance of the devices is attributed to the improved photophysical properties in neat film due to functionalization of fluoranthene core. The reduction in molecular aggregation and tuning of the molecular energy level has been achieved by substituents on the periphery on fluoranthene core. The color purity and performance of the device further may get improved with the optimization of the device structure.

Experimental

Materials

1,3-Diphenyl-2-propanone, acenaphthenequinone, phenylacetylene, 4-iodobenzonitrile, 4-iodotoluene, 4-iodophenol, ethynyltrimethylsilane, bis(triphenylphosphine)palladium(II) dichloride were purchased from Sigma-Aldrich Co. LLC and used as received without any further purification. Triethylamine was dried over sodium hydroxide prior to use. High pressure Teflon coated sealed tubes were used for synthesis. Diphenyl ether was purchased from S D Fine-Chemicals Limited.

Synthesis

All the fluoranthene derivatives were synthesized according to the scheme outlined in Scheme 1**.** Synthesis of different substituted diphenylacetylene derivatives and desired fluoranthene derivatives is described in supporting information.

Characterization

The reaction products and their purity were confirmed with NMR spectroscopy, mass spectrometry and elemental analysis. ^{1}H and ^{13}C NMR spectra were recorded on Bruker 400 MHz and 100 MHz spectrometer, respectively, and calibrated using TMS as an internal reference. Chemical shifts are reported in parts per million (ppm). Mass spectra were recorded on Thermo LCQ Deca XP Max by electrospray ionization (ESI) technique. Elemental analysis was carried out on Thermo Scientific Flash 2000 Organic Elemental Analyzer. The UV-visible absorption spectra were obtained with a Perkin-Elmer (Lambda 35) UV-visible spectrometer. All the absorption spectra in the solution state were recorded in optical grade chloroform (conc. $1x10^{-5}$ M), and the spectra in solid state were recorded from films of compounds spin coated on quartz substrate. Steady-state fluorescence emission spectra were recorded on Horiba Jobin-YvonFluoroLog-3 spectrometer. The transient PL decay characteristics were recorded with time correlated single photon counting (TCSPC) method using LED 365 nm with a Quantaurus-Tau fluorescence lifetime measurement system (C11367-03, Hamamatsu Photonics Co.). The fluorescence emission decay was well fitted by a single exponential decay profile. Absolute photoluminescence quantum yields (PLQY) were obtained using a Quantaurus-QY measurement system (C11347-11, Hamamatsu Photonics Co.). Single crystal X-ray diffraction data sets were collected on an Oxford Xcalibur (Mova) diffractometer equipped with a EOS CCD detector and Bruker D8Quest with CMOS detector using Mo K_α radiation (λ= 0.71073Å). The single crystal was maintained at the desired temperature during data collection using the Oxford instruments Cryojet-HT controller. All structures were solved by direct methods and refined using SHELXL-97.[46] H-atoms were fixed geometrically and refined isotropically. The WinGX package was used for refinement and production of data tables along with and ORTEP diagram for structure visualization and making molecular representations.[47] Analysis of the H-bonding and π-π interactions were carried out using PLATON and packing diagrams were generated by using MERCURY.[48] All quantum chemical calculations were carried out in Gaussian 09 Program by using the hybrid function M062X with 3-21G basis set.[49] Differential Scanning Calorimetry (DSC) analysis was carried out on Mettler Toledo DSC1 STARe system (chiller cooled) with N_2 flow of 40 mL/min with an empty Al pan taken as standard. All samples were heated up at a heating rate of 5 °C/min. Redox potentials were determined by cyclic voltammetry (CV) experiment using CH electrochemical analyser with scanning rate of 50 mV/s. Synthesized materials (0.2 mg/ 0.1 mL DCM) were drop casted on working Pt disc electrode. Ag/AgCl was used as a reference electrode whereas Pt wire was employed as counter electrodes. Dry chloroform and 0.1 M tetrabutylammonium hexafluorophosphate were used as solvent and supporting electrolyte, respectively. Ferrocene/ferrocenium (Fc/Fc^{+}) (HOMO=-4.80 eV) couple was used as standard electrochemical reference.[50]

Conclusion

In summary, we have synthesized fluoranthene derivatives with various donor and acceptor substituents *via* Diels-Alder reaction of 7,9-diphenyl-8*H*-cyclopenta[*a*]acenaphthylen-8-one with appropriate acetylene derivatives. The single crystal studies perceive the various intermolecular interactions between the molecules and improved the understanding of the optical and thermal properties of this class of molecules. Computational studies further supported the experimental findings. Finally, the multilayer non-doped OLED devices were fabricated and sky blue to bluish green color was observed. Our study presents a systematic approach of molecular design to tune the color of fluoranthene based derivatives.

Acknowledgement

We acknowledge science and engineering research board, Department of Science and Technology for supporting this work through the project EMR/2015/000969. Authors thank Prof. Chihaya Adachi and Dr. Qisheng Zhang for useful discussion and providing facility for OLED device fabrication and characterization. Authors also thank NMR Research Centre, IISc for NMR facility. Shiv Kumar acknowledges Dr. Sathya Perumal for useful discussion on theoretical study and University Grant Commission (UGC) for junior research fellowship (JRF).

Notes and references

[a] Solid State and Structural Chemistry Unit, Indian Institute of Science, Bangalore 560012, India.

[b] Inorganic and Physical chemistry, Indian Institute of Science, Bangalore 560012, India. Present Address: Department of Chemistry, Central University of Karnataka, Kalaburagi 585367, Karnataka, India.

*Corresponding Author - satish@sscu.iisc.ernet.in

The authors declare no competing financial interest.

Electronic Supplementary Information (ESI) available: detail of the synthetic procedures, ^{1}H and ^{13}C NMR, mass spectra, ORTEP diagram, cyclic voltammograms and summary of torsion angles. See DOI: 10.1039/b000000x/

1. M. Pope, H. Kallmann and P. Magnante, *J. Chem. Phys.*, 1963, **38**, 2042-2043.
2. W. Helfrich and W. Schneider, *Phys. Rev. Lett.*, 1965, **14**, 229.
3. W. Helfrich and W. Schneider, *J. Chem. Phys.*, 1966, **44**, 2902-2909.
4. C. W. Tang and S. Van Slyke, *Appl. Phys. Lett.*, 1987, **51**, 913-915.
5. K. T. Kamtekar, A. P. Monkman and M. R. Bryce, *Adv. Mater.*, 2010, **22**, 572-582.
6. G. M. Farinola and R. Ragni, *Chem. Soc. Rev.*, 2011, **40**, 3467-3482.
7. H. Sasabe and J. Kido, *J. Mater. Chem. C*, 2013, **1**, 1699-1707.

8. P. E. Burrows, G. Gu, V. Bulovic, Z. Shen, S. R. Forrest and M. E. Thompson, *Electron Devices, IEEE Transactions on*, 1997, **44**, 1188-1203.
9. Y.-H. Chung, L. Sheng, X. Xing, L. Zheng, M. Bian, Z. Chen, L. Xiao and Q. Gong, *J. Mater. Chem. C*, 2015, **3**, 1794-1798.
10. Y. J. Pu, G. Nakata, F. Satoh, H. Sasabe, D. Yokoyama and J. Kido, *Adv. Mater.*, 2012, **24**, 1765-1770.
11. S. Zhang, L. Yao, Q. Peng, W. Li, Y. Pan, R. Xiao, Y. Gao, C. Gu, Z. Wang, P. Lu, F. Li, S. Su, B. Yang and Y. Ma, *Adv. Funct. Mater.*, 2015, **25**, 1755-1762.
12. H. Xiao, L. Ding, D. Ruan, B. Li, N. Ding and D. Ma, *Dyes and Pigments*, 2015, **121**, 7-12.
13. C.-L. Liu, C.-J. Zheng, X.-K. Liu, Z. Chen, J.-P. Yang, F. Li, X.-M. Ou and X.-H. Zhang, *J. Mater. Chem. C*, 2015, **3**, 1068-1076.
14. G. Mallesham, C. Swetha, S. Niveditha, M. E. Mohanty, N. J. Babu, A. Kumar, K. Bhanuprakash and V. J. Rao, *J. Mater. Chem. C*, 2015, **3**, 1208-1224.
15. C. Adachi, T. Tsutsui and S. Saito, *Appl. Phys. Lett.*, 1990, **56**, 799-801.
16. S. Tao, Z. Peng, X. Zhang, P. Wang, C. S. Lee and S. T. Lee, *Adv. Funct. Mater.*, 2005, **15**, 1716-1721.
17. K. S. Kim, Y. M. Jeon, J. W. Kim, C. W. Lee and M. S. Gong, *Org. Electron.*, 2008, **9**, 797-804.
18. A. L. Kanibolotsky, R. Berridge, P. J. Skabara, I. F. Perepichka, D. D. Bradley and M. Koeberg, *J. Am. Chem. Soc.*, 2004, **126**, 13695-13702.
19. C. C. Yeh, M. T. Lee, H. H. Chen and C. H. Chen, in *SID Symposium*, 2004, p. 788.
20. X. K. Liu, Z. Chen, C. J. Zheng, M. Chen, W. Liu, X. H. Zhang and C. S. Lee, *Adv. Mater.*, 2015, **27**, 2025-2030.
21. R. Holmes, B. D'Andrade, S. Forrest, X. Ren, J. Li and M. Thompson, *Appl. Phys. Lett.*, 2003, **83**, 3818-3820.
22. S. Tao, S. Xu and X. Zhang, *Chem. Phys. Lett.*, 2006, **429**, 622-627.
23. C. Adachi, M. A. Baldo, M. E. Thompson and S. R. Forrest, *J. Appl. Phys.*, 2001, **90**, 5048-5051.
24. Y.-C. Tsai and J.-H. Jou, *Appl. Phys. Lett.*, 2006, **89**, 243521.
25. P. I. Shih, C. Y. Chuang, C. H. Chien, E. G. Diau and C. F. Shu, *Adv. Funct. Mater.*, 2007, **17**, 3141-3146.
26. J. Huang, N. Sun, J. Yang, R. Tang, Q. Li, D. Ma, J. Qin and Z. Li, *J. Mater. Chem.*, 2012, **22**, 12001-12007.
27. Y. H. Kim, H. C. Jeong, S. H. Kim, K. Yang and S. K. Kwon, *Adv. Funct. Mater.*, 2005, **15**, 1799-1805.
28. E. J. List, R. Guentner, P. Scanducci de Freitas and U. Scherf, *Adv. Mater.*, 2002, **14**, 374-378.
29. K.-T. Wong, Y.-Y. Chien, R.-T. Chen, C.-F. Wang, Y.-T. Lin, H.-H. Chiang, P.-Y. Hsieh, C.-C. Wu, C. H. Chou and Y. O. Su, *J. Am. Chem. Soc.*, 2002, **124**, 11576-11577.
30. E. W. Thulstrup and J. Eggers, *Chem. Phys. Lett.*, 1968, **1**, 690-692.
31. I. B. Berlman, H. O. Wirth and O. Steingraber, *J. Am. Chem. Soc.*, 1968, **90**, 566-569.
32. B. Nickel, *Chem. Phys. Lett.*, 1974, **27**, 84-90.
33. X.-J. Li, M. Li, W. Yao, H.-Y. Lu, Y. Zhao and C.-F. Chen, *RSC Advances*, 2015, **5**, 18609-18614.
34. A. Goel, V. Kumar, S. Chaurasia, M. Rawat, R. Prasad and R. Anand, *The Journal of organic chemistry*, 2010, **75**, 3656-3662.
35. R. C. Chiechi, R. J. Tseng, F. Marchioni, Y. Yang and F. Wudl, *Adv. Mater.*, 2006, **18**, 325-328.
36. S. K. Kim, J. Y. Jaung and J. W. Park, *Mol. Cryst. Liq. Cryst.*, 2008, **491**, 122-132.
37. S. K. Kim and J. W. Park, *J. Nanosci. Nanotech.*, 2008, **8**, 4787-4792.
38. N. Kapoor and K. J. Thomas, *New J. Chem.*, 2010, **34**, 2739-2748.
39. Y. H. Lee, T. C. Wu, C. W. Liaw, T. C. Wen, T. F. Guo and Y. T. Wu, *J. Mater. Chem.*, 2012, **22**, 11032-11038.
40. Y. H. Lee, T. C. Wu, C. W. Liaw, T. C. Wen, S. W. Feng, J. J. Lee, Y. T. Wu and T. F. Guo, *Org. Electron.*, 2013, **14**, 1064-1072.
41. Y. Yuan, J.-X. Chen, F. Lu, Q.-X. Tong, Q.-D. Yang, H.-W. Mo, T.-W. Ng, F.-L. Wong, Z.-Q. Guo and J. Ye, *Chem. Mater.*, 2013, **25**, 4957-4965.
42. W. Walker, B. Veldman, R. Chiechi, S. Patil, M. Bendikov and F. Wudl, *Macromolecules*, 2008, **41**, 7278-7280.
43. K. Sonogashira, Y. Tohda and N. Hagihara, *Tetrahedron Lett.*, 1975, **16**, 4467-4470.
44. J. Shi and C. W. Tang, *Appl. Phys. Lett.*, 2002, **80**, 3201-3203.
45. H. Z. Xie, M. W. Liu, O. Y. Wang, X. H. Zhang, C. S. Lee, L. S. Hung, S. T. Lee, P. F. Teng, H. L. Kwong, H. Zheng and C. M. Che, *Adv. Mater.*, 2001, **13**, 1245-1248.
46. G. M. Sheldrick, *Acta Crystallogr. Sect. A: Found. Crystallogr.*, 2007, **64**, 112-122.
47. L. J. Farrugia, *J. Appl. Crystallogr.*, 1997, **30**, 565-565.
48. L. J. Farrugia, *J. Appl. Crystallogr.*, 1999, **32**, 837-838.
49. M. Frisch, G. Trucks, H. Schlegel, G. Scuseria, M. Robb, J. Cheeseman, J. Montgomery, T. Vreven, K. Kudin and J. Burant, 2008.
50. C. M. Cardona, W. Li, A. E. Kaifer, D. Stockdale and G. C. Bazan, *Adv. Mater.*, 2011, **23**, 2367-2371.